

Structural, magnetic, and electrical properties of spin coated ilmenite-pseudobrookite $x\text{FeTiO}_3\text{-(1-x)Fe}_2\text{O}_3$ thin films

A. Dixit, S. Putatunda, R. Suryanarayanan, and R. Naik

Citation: *Journal of Applied Physics* **122**, 103901 (2017); doi: 10.1063/1.4986874

View online: <http://dx.doi.org/10.1063/1.4986874>

View Table of Contents: <http://aip.scitation.org/toc/jap/122/10>

Published by the [American Institute of Physics](#)

Articles you may be interested in

[Electronic properties of lithiated SnO-based anode materials](#)

Journal of Applied Physics **122**, 055105 (2017); 10.1063/1.4997539

[Effects of Ce doping and humidity on UV sensing properties of electrospun ZnO nanofibers](#)

Journal of Applied Physics **122**, 105102 (2017); 10.1063/1.5000443

[Low-temperature magnetic behavior of nanostructured ferrite compositions prepared by plasma spraying](#)

Journal of Applied Physics **122**, 104103 (2017); 10.1063/1.5001506

[Cs diffusion in SiC high-energy grain boundaries](#)

Journal of Applied Physics **122**, 105901 (2017); 10.1063/1.4989389

[Enhanced magnetization in morphologically and magnetically distinct \$\text{BiFeO}_3\$ and \$\text{La}_{0.7}\text{Sr}_{0.3}\text{MnO}_3\$ composites](#)

Journal of Applied Physics **122**, 104101 (2017); 10.1063/1.5001566

[Optical switching of a graphene mechanical switch using the Casimir effect](#)

Journal of Applied Physics **122**, 104501 (2017); 10.1063/1.4993672

HIDEN
ANALYTICAL

Instruments for Advanced Science

Contact Hiden Analytical for further details:

W www.HidenAnalytical.com
E info@hiden.co.uk

CLICK TO VIEW our product catalogue



Gas Analysis

- dynamic measurement of reaction gas streams
- catalysis and thermal analysis
- molecular beam studies
- dissolved species probes
- fermentation, environmental and ecological studies



Surface Science

- LEIS/TPD
- SIMS
- end point detection in ion beam etch
- elemental imaging, surface mapping



Plasma Diagnostics

- plasma source characterization
- etch and deposition process reaction
- kinetic studies
- analysis of neutral and radical species



Vacuum Analysis

- partial pressure measurement and control of process gases
- reactive sputter process control
- vacuum diagnostics
- vacuum coating process monitoring

Structural, magnetic, and electrical properties of spin coated ilmenite-pseudobrookite $x\text{FeTiO}_3-(1-x)\text{Fe}_2\text{O}_3$ thin films

A. Dixit,^{1,2,a)} S. Putatunda,¹ R. Suryanarayanan,^{1,3} and R. Naik¹

¹Department of Physics and Astronomy, Wayne State University, Detroit, Michigan 48201, USA

²Department of Physics and Center for Solar Energy, Indian Institute of Technology, Jodhpur 342011, Rajasthan, India

³Laboratoire de Physico-Chimie de l'Etat Solide, ICMMO, CNRS, UMR 8648, Université Paris-Sud, 91405 Orsay, France

(Received 7 June 2017; accepted 25 August 2017; published online 8 September 2017)

We report on the structural, magnetic, optical, and electrical properties of iron titanate thin films prepared using a spin-coating technique having nominal compositions of FeTiO_3 and $\text{Fe}_{1.4}\text{Ti}_{0.6}\text{O}_3$. X-ray diffraction measurements show clear evidence for the presence of both ilmenite and pseudobrookite crystal structures, which is confirmed using Raman spectroscopy. X-ray photoemission spectroscopy studies indicate that Fe is present mainly in the 2+ valence state, with some Fe^{3+} present on the more heavily oxidized surface of the films. The as-prepared samples exhibit weak ferromagnetism at room temperature. While the valence state of Fe is not significantly affected by vacuum annealing, the saturation magnetization is increased dramatically, reaching nearly 220 emu mole⁻¹ for the Fe-rich film. The optical band gap was found to be roughly 2.0 eV for all samples, with negligible changes on vacuum annealing. *Published by AIP Publishing.*

[<http://dx.doi.org/10.1063/1.4986874>]

INTRODUCTION

Spintronic devices use electron spin together with electron charge to store and manipulate information, allowing more versatile applications.¹ There has been a great deal of interest in developing new materials for spintronic devices based on ferromagnetic semiconducting oxides, including transition metal doped TiO_2 and ZnO .²⁻¹¹ These materials typically have magnetic ordering temperatures above room temperature, enabling them to be readily incorporated into devices. A number of recent studies have postulated that oxygen vacancies may be a necessary ingredient for promoting this room temperature ferromagnetism in some of these materials.^{12,13} One particularly interesting dilute magnetic semiconductor is the solid solution of ilmenite (FeTiO_3) and hematite ($\alpha\text{-Fe}_2\text{O}_3$). While hematite is antiferromagnetic, solid solutions of FeTiO_3 and $\alpha\text{-Fe}_2\text{O}_3$ are ferromagnetic.¹⁴ The ferromagnetic order has been attributed to the mixture of Fe^{2+} and Fe^{3+} states at the interface between the hematite and ilmenite phases.¹⁵⁻¹⁷ The solid solution $x\text{FeTiO}_3-(1-x)\text{Fe}_2\text{O}_3$ (also written as $\text{Fe}_{2-x}\text{Ti}_x\text{O}_3$), having the ilmenite $R\bar{3}$ space group, is expected to exhibit ferromagnetic properties in the range $0.5 < x < 0.85$.^{18,19} Furthermore, this system allows for the development of both n- and p-type semiconductors by controlling the $\alpha\text{-Fe}_2\text{O}_3$ concentration,²⁰ with pure FeTiO_3 being an intrinsic p-type semiconductor with a bulk band gap of 2.6 eV,²¹ although larger values are reported for thin film samples.²²

Utilizing ilmenite-hematite solutions for many device applications will require preparing the materials in thin film geometries. Previous techniques used for depositing high quality FeTiO_3 thin films include sputtering²³ and pulsed

laser deposition.²⁴ Spin coating can provide a simpler method for preparing films of both iron titanate and iron titanate/iron oxide films, potentially at the expense of somewhat lower quality samples, as secondary phases of different iron titanium oxides can develop over a range of post-preparation treatments. In particular, ilmenite films are sensitive to the annealing temperature and the atmosphere, and can express a number of different structures.^{25,26} Of these, the (ferric) pseudobrookite phase (Fe_2TiO_5) has been shown to be the most stable structure at temperatures above 1173 K.²⁷ Impurity phases have also been shown to arise with changes in composition, with an increase in the iron fraction leading to a mixture of ilmenite and pseudobrookite phases with sol-gel synthesis.^{28,29} While the pseudobrookite phase is non-magnetic at room temperature, it develops a novel anisotropic spin glass state³⁰ approximately below $T_G = 50$ K. Pseudobrookite structures having the composition FeTi_2O_5 may also develop as impurity phases^{31,32} even at intermediate temperatures.

Motivated by the observation that the pseudobrookite structure readily develops as an impurity phase in ilmenite films, the purpose of this investigation is to probe the magnetic and electrical properties of mixed phase ilmenite-pseudobrookite films. This particular system has also been studied for applications to rad-hard electronics.³³ Previous work on ilmenite-hematite solid solutions has established the importance of having a mixed Fe valence at the interface between different phases to produce a large magnetization.^{15,17} While the identical mechanism for weak ferromagnetism may not be relevant for ilmenite-pseudobrookite composites, as the crystal structures across the interface are different, the fact that ferric pseudobrookite contains Fe in the 3+ state allows some possibility of similar induced lamellar magnetism. Furthermore, oxygen vacancy defects, believed to

a) ambesh@iitj.ac.in

be required for the development of room temperature ferromagnetism in many semiconducting oxides, may be stabilized at the interfaces between the ilmenite and pseudobrookite structures. In order to explore the effects of interfaces in these iron titanium oxide materials, we have characterized the magnetic, electrical, and optical properties of nominally stoichiometric FeTiO_3 and iron-rich $\text{Fe}_{1.4}\text{Ti}_{0.6}\text{O}_3$ thin films, under conditions of both air and vacuum annealing.

EXPERIMENTAL METHOD

Iron titanium oxide thin films were synthesized using a spin coating technique. The samples were prepared starting from organic precursors, iron (III)-2 ethylhexanoate and titanium (IV)-2 ethylhexanoate, to produce solutions having the desired ratios of 1:1 and 1.4:0.6 for iron to titanium. These organic solutions were deposited dropwise on single crystal silicon or c-axis oriented sapphire substrates, which were then rotated at 5000 rpm. The organic constituents were burned off by annealing in air at 500°C for 1 min, with each film having a total of 10 coats corresponding to a total thickness of roughly $1\ \mu\text{m}$. The as-deposited films were then annealed in air for 1 h at 900°C to crystallize in the desired phase. In order to study the effects of oxygen vacancy defects on the properties of these FeTiO_3 films, some samples were annealed under high vacuum ($\sim 10^{-7}$ Torr) at 600°C for 3 h.

RESULTS AND DISCUSSION

The crystal structure of the films was investigated using X-ray diffraction (XRD) spectra recorded using a Rigaku diffractometer. Figure 1(a) plots the diffraction peaks for the same FeTiO_3 thin film sample deposited on sapphire and annealed under both air and vacuum, with the y-axis intensity scales being offset for clarity. These diffraction patterns show the presence of the ilmenite phase, together with the peaks expected for the pseudobrookite (Fe_2TiO_5 or FeTi_2O_5) structure. The XRD spectra are qualitatively similar for the air and vacuum annealed (VA) samples, suggesting that vacuum annealing does not promote the development of additional impurity phases. In particular, there is no evidence for the formation of any crystalline magnetic iron oxide impurity phase on vacuum annealing. The XRD patterns for the

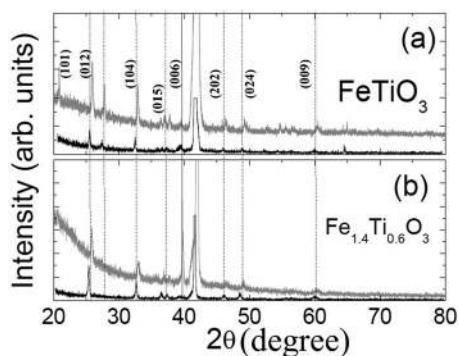


FIG. 1. X-ray diffraction spectra of the (a) FeTiO_3 and (b) $\text{Fe}_{1.4}\text{Ti}_{0.6}\text{O}_3$ films, for both the as-prepared (lower trace) and vacuum annealed (upper trace) samples. The dashed lines indicate the position of the diffraction peaks expected for ilmenite and pseudobrookite structures.

$\text{Fe}_{1.4}\text{Ti}_{0.6}\text{O}_3$ films, both air and vacuum annealed, are shown in Fig. 1(b). These diffraction peaks can also be indexed to a mixture of ilmenite and pseudobrookite structures, although we are unable to quantitatively determine whether the volume fractions of these two phases are similar to those in the stoichiometric FeTiO_3 films. The observed diffraction peaks are marked with the respective (h k l) planes, and the results are in agreement with the reference XRD pattern (ICDD PDF # 791838).

We used Raman spectroscopy as a more sensitive probe to detect possible impurity phases in these samples. These spectra were acquired at room temperature using a Triax spectrometer with a J.Y. Horiba microscope with an Ar^+ -ion laser at 514.5 nm. The collection time was fixed at 10 s for all measurements, at a fixed laser power of approximately 8 mW on the sample. Figure 2(a) shows the Raman spectra for both the air and vacuum annealed FeTiO_3 films, while Fig. 2(b) plots similar Raman data for the $\text{Fe}_{1.4}\text{Ti}_{0.6}\text{O}_3$ sample. We find that both compositions show peaks expected for both the pseudobrookite and ilmenite phases,²⁸ as indicated in Fig. 2. The observed vibrational modes at ~ 200 , 225, 335, 445, 610 and $660\ \text{cm}^{-1}$ correspond to the FeTiO_3 sample.³⁶ Similar modes are also observed for $\text{Fe}_{1.4}\text{Ti}_{0.6}\text{O}_3$ sample, suggesting the absence of any major impurities in these samples. However, there is a small additional peak near $300\ \text{cm}^{-1}$ for the $\text{Fe}_{1.4}\text{Ti}_{0.6}\text{O}_3$ sample. This can be attributed to hematite, which has been shown to develop in Fe-rich iron titanates.²⁸ Although the absolute intensity of the signal changes between the air and vacuum annealed samples, the peak positions are unchanged, and no new peaks develop on vacuum annealing. This is consistent with the XRD data, which suggest that no new impurity phases develop on vacuum annealing.

We also conducted X-ray photoelectron spectroscopy (XPS) studies to characterize the composition of and the electronic valence states in these thin films. We plot the measured elemental XPS plots for Fe 2p, Ti 2p and O 1s for both FeTiO_3 and $\text{Fe}_{1.4}\text{Ti}_{0.6}\text{O}_3$ vacuum annealed (VA) and air annealed (AA) films in Figs. 3 and 4 respectively. Figures 3(c) and 3(d) show the Fe 2p XPS spectra after sputtering with argon to remove the surface layer to a depth of approximately 15 nm. The XPS spectra for the binding energies

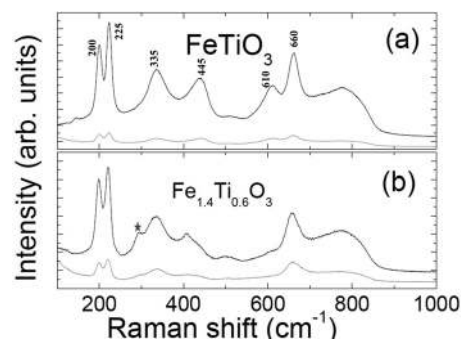


FIG. 2. Raman spectra of the (a) FeTiO_3 and (b) $\text{Fe}_{1.4}\text{Ti}_{0.6}\text{O}_3$ films, for both the as-prepared (upper trace) and vacuum annealed (lower trace) samples. The peaks expected for the ilmenite (I) and pseudobrookite (P) phases are indicated. The small peak marked by an asterisk (*) for the $\text{Fe}_{1.4}\text{Ti}_{0.6}\text{O}_3$ film is attributed to a small hematite secondary phase.

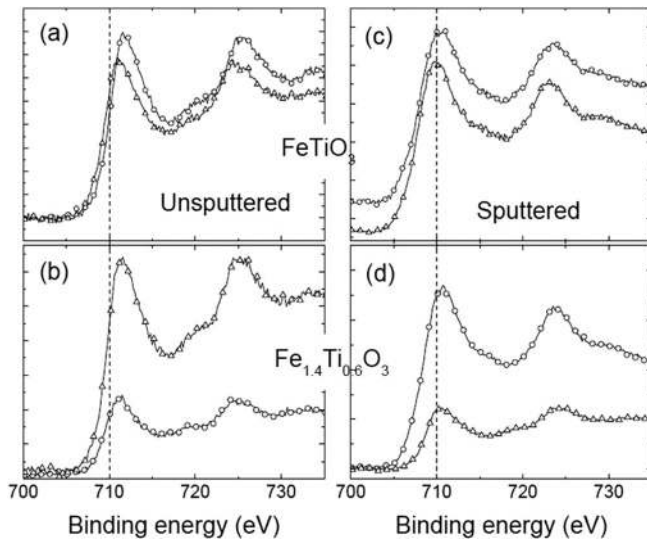


FIG. 3. X-ray photoemission spectra near the Fe edge of the (a) FeTiO_3 and (b) $\text{Fe}_{1.4}\text{Ti}_{0.6}\text{O}_3$ films, for both the as-prepared (triangles) and vacuum annealed (circles) samples. Panels (c) and (d) show the XPS spectra for the films after sputtering with Ar to remove the surface of the sample. The dashed line is for guiding the eye.

associated with Ti and O showed negligible changes in sputtering, and are not included.

The Fe 2P XPS spectra measured at the film surfaces show features consistent with a mixture of 2+ and 3+ valence states. The Fe $2p_{3/2}$ peak falls near 711.2 eV, which is typical for a 3+ valence, but the width of the peak suggests some admixture of Fe^{2+} ,²³ which exhibits a peak at slightly lower binding energies. The broad feature near 718 eV is attributed to a weak shake-up satellite peak for Fe^{3+} .³⁴ On vacuum annealing, the binding energies of the FeTiO_3 film shift to slightly lower energies, more consistent with a 2+ valence, while the 718 eV shake-up peak drops in intensity. $\text{FeTiO}_{3+\delta}$ films having an excess of oxygen are observed to have a strong Fe^{3+} signal in XPS, while films having a stoichiometric oxygen content show peaks expected for

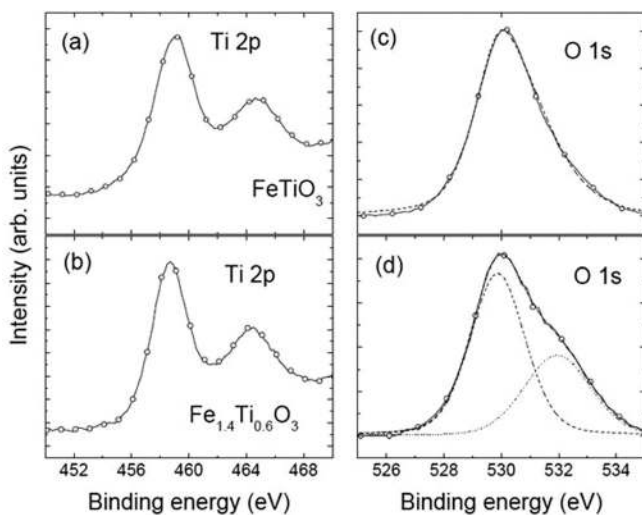


FIG. 4. X-ray photoemission spectra of the as-prepared films (a) near the Ti edge for FeTiO_3 , (b) near the Ti edge for $\text{Fe}_{1.4}\text{Ti}_{0.6}\text{O}_3$, (c) near the O edge for FeTiO_3 , and (d) near the O edge for $\text{Fe}_{1.4}\text{Ti}_{0.6}\text{O}_3$. The dashed lines in panel (d) show the fit to the O peak, as described in the text.

Fe^{2+} .²³ Thus, a change in Fe valence from 3+ to 2+ is consistent with a reduction in the oxygen content of the films. After sputtering with Ar, the Fe $2p_{3/2}$ binding energy falls closer to 710 eV, which is attributed to Fe in the 2+ state, and the Fe^{3+} shake-up peak near 718 eV is much smaller or absent completely. These measurements suggest that while the surfaces of the films may be oxidized under ambient conditions, leading to Fe being present in both the 2+ and 3+ valence states, below this surface layer, the samples consist of nearly stoichiometric FeTiO_3 or FeTi_2O_5 , with the ferric pseudobrookite (Fe_2TiO_5), which has Fe present in the 3+ state being mostly absent.

The Ti 2p peak, shown in Fig. 4, falls near 458.5 eV for both the FeTiO_3 and $\text{Fe}_{1.4}\text{Ti}_{0.6}\text{O}_3$ films, indicating that Ti is present only in the 4+ valence. This is expected, since both ilmenite and pseudobrookite contain Ti in the 4+ state. Furthermore, the Ti valence does not change under vacuum annealing. The O1s peak is at 530.5 eV for the FeTiO_3 film for both the air annealed and vacuum annealed samples, while two peaks at 530 eV and 532 eV are needed to fit the spectrum in $\text{Fe}_{1.4}\text{Ti}_{0.6}\text{O}_3$, as shown in Fig. 4. This implies that there are two separate environments for oxygen in the $\text{Fe}_{1.4}\text{Ti}_{0.6}\text{O}_3$ films. The specific origin of these two different binding energies is unclear, but a similar peak in the oxygen XPS trace near 532 eV has previously been identified with OH complexes.³⁵

We measured the magnetic characteristics of these films using a Quantum Design superconducting quantum interference device (MPMS). The room temperature magnetic hysteresis measurements were performed at fields of up to $H = 50$ kOe, and we estimated the diamagnetic contribution of the substrate from the high-field magnetization. The magnetization curves corrected for the estimated substrate contribution, for the air annealed and vacuum annealed FeTiO_3 films, are shown in Fig. 5(a). The air annealed sample shows a saturation magnetization of 17 emu/mol, which increases to approximately 100 emu/mole for the vacuum annealed sample. The magnetic hysteresis is small for the air annealed sample, with coercivity of the order of only 250 Oe, which increases remarkably to 8 kOe on vacuum annealing. In the absence of secondary phases, the $x = 1$ composition of $\text{Fe}_{2-x}\text{Ti}_x\text{O}_3$ is not expected to exhibit any ferromagnetism. However, weak ferromagnetism is commonly observed in many semiconducting oxides, and can be associated with oxygen vacancies.¹² The small moment in the as-prepared sample can be attributed to residual oxygen vacancy defects at the ilmenite-pseudobrookite interface, with the dramatic increase in the saturation magnetization on vacuum annealing being associated with the introduction of additional oxygen vacancies.

Qualitatively, very similar behaviour is observed in the magnetization curves for the air and vacuum annealed $\text{Fe}_{1.4}\text{Ti}_{0.6}\text{O}_3$ films, as shown in Fig. 5(b), for which the saturation moment increases from 12 emu/mole(Fe) to roughly 220 emu/mole(Fe). This large saturation magnetization corresponds to an effective moment of $0.04 \mu_B$ per Fe ion. Previous studies on the $x = 0.6$ composition,¹⁹ consisting of mixed ilmenite and hematite phases, find saturation magnetic moments of approximately $0.3 \mu_B/\text{f.u.}$ at 300 K. This suggests

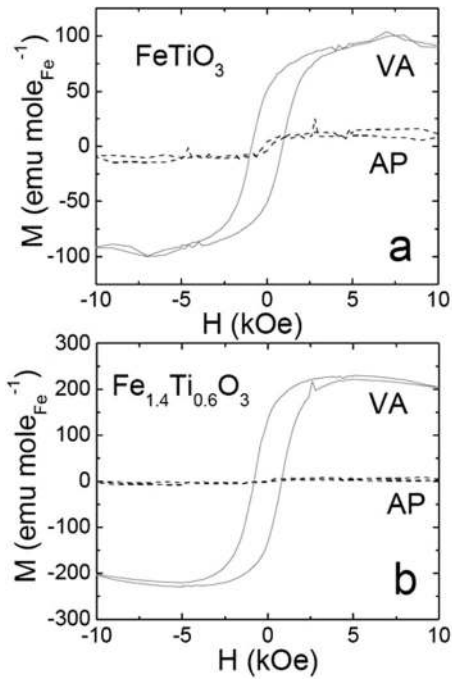


FIG. 5. $M(H)$ curves measured at room temperature for (a) FeTiO_3 and (b) $\text{Fe}_{1.4}\text{Ti}_{0.6}\text{O}_3$, for both the as-prepared (AP) air annealed samples and vacuum annealed (VA) samples.

that while oxygen vacancy defects can produce weak ferromagnetism in ilmenite-pseudobrookite films, the magnetization produced by this mechanism is roughly an order of magnitude smaller than the lamellar magnetism developing in the mixed valence ilmenite-hematite structure. We believe that the large room saturation moment, we observe, cannot be simply attributed to some non- or weakly-magnetic iron oxide impurity in the as-prepared sample that develops a sizeable moment which reduced on vacuum annealing. We find no evidence for additional phase development, or disappearance, on vacuum annealing in either the XRD measurements or Raman spectra. Furthermore, XPS measurements of the samples show no evidence for any Fe^0 states in the vacuum annealed samples.

Varying the Fe:Ti ratio and, especially, introducing oxygen vacancy defects is expected to strongly affect the electrical properties of iron titanate films. In order to determine the carrier concentrations and mobilities of the films, we conducted room temperature Hall effect measurements using a standard 4-probe configuration having gold wires attached to silver contacts with the application of a $H = 10$ kOe magnetic field. The air annealed samples were too resistive to be investigated using this apparatus, but the samples became much more conducting on vacuum annealing. The n-type carrier concentration for the vacuum annealed FeTiO_3 film was estimated to be roughly $10^{16}/\text{cm}^3$ with a mobility of $30 \text{ cm}^2 \text{ V}^{-1} \text{ s}^{-1}$. For the vacuum annealed $\text{Fe}_{1.4}\text{Ti}_{0.6}\text{O}_3$ sample, we obtained an n-type carrier concentration of approximately $10^{17}/\text{cm}^3$ and a mobility of $6 \text{ cm}^2 \text{ V}^{-1} \text{ s}^{-1}$. The conductivity values are ~ 48 and $\sim 100 \text{ m}\Omega^{-1} \text{ cm}^{-1}$ for FeTiO_3 and $\text{Fe}_{1.4}\text{Ti}_{0.6}\text{O}_3$ VA samples respectively.

We measured optical spectra to investigate the electronic structure and determine the absorption edge for the

FeTiO_3 and $\text{Fe}_{1.4}\text{Ti}_{0.6}\text{O}_3$ films prepared on sapphire substrates. The optical transmission and reflectance data were collected from 3300 nm to 200 nm using a Perkin-Elmer Lambda 300 UV-Vis-NIR optical spectrometer. We used these transmittance and reflectance data to estimate the optical absorption coefficient α . We plot $(\alpha E)^2$ against energy for both the air annealed (AA) and vacuum annealed (VA) FeTiO_3 and $\text{Fe}_{1.4}\text{Ti}_{0.6}\text{O}_3$ films in Figs. 6(a) and 6(b) respectively. The optical bandgap is found to be approximately 2.0 eV for both FeTiO_3 and $\text{Fe}_{1.4}\text{Ti}_{0.6}\text{O}_3$ samples, which is lower than the previously reported values.²¹ We do not observe any discernible change in the optical band gap after vacuum annealing of these samples, suggesting that there is no significant Burstein-Moss shift. This is consistent with our electrical measurements, where we found only a small increase in the carrier concentration after vacuum annealing. In this respect, the ilmenite-pseudobrookite films are unlike some other oxide semiconducting films, where vacuum annealing can produce a significant increase in the carrier concentration, which substantially modifies the optical spectrum.¹³

Taken together, these data suggest that room temperature ferromagnetism may be developing in these ilmenite-pseudobrookite films. Rather surprisingly, the films seem to consist of an admixture of FeTiO_3 and FeTi_2O_5 , both having Fe in the 2+ valence, with no clear evidence for Fe_2TiO_5 being present, even in the Fe-rich $\text{Fe}_{1.4}\text{Ti}_{0.6}\text{O}_3$ sample. The larger magnetization observed in the $\text{Fe}_{1.4}\text{Ti}_{0.6}\text{O}_3$ sample can perhaps be attributed to some trace $\alpha\text{-Fe}_2\text{O}_3$ phase observed in the Raman spectra, which is absent in FeTiO_3 . This suggests that the mechanism for the onset of room temperature magnetism is not solely lamellar ferromagnetism, as in ilmenite-hematite structures, because there is no mixture of Fe^{2+} and Fe^{3+} states at the interface between the FeTiO_3 and FeTi_2O_5 crystallites in the FeTiO_3 films, although this effect

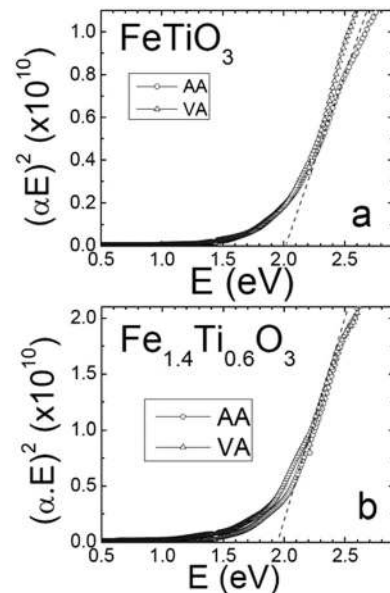


FIG. 6. Optical absorption spectra of (a) FeTiO_3 and (b) $\text{Fe}_{1.4}\text{Ti}_{0.6}\text{O}_3$, for both the as-prepared and air annealed samples. The dashed line shows the extrapolation of the absorption curve used to estimate the band gap.

may provide some additional contributions for the $\text{Fe}_{1.4}\text{Ti}_{0.6}\text{O}_3$ sample. While the magnetization in both films shows a dramatic increase on vacuum annealing, the size of the magnetic moment remains roughly an order of magnitude smaller than that observed in ilmenite-hematite samples. This implies that while oxygen vacancies can produce a sizable magnetization in ilmenite-pseudobrookite composites, much higher magnetization develops in ilmenite-hematite structures due to the presence of a mixed Fe valence at the interfaces.¹⁵ One possible approach for increasing the magnetization in ilmenite-pseudobrookite films would be stabilizing the ferric pseudobrookite phase, Fe_2TiO_5 , since the iron in this structure is present in the Fe^{3+} state.

CONCLUSION

In conclusion, we find that our iron titanate films deposited by spin coating contain an admixture of ilmenite and pseudobrookite structures. Based on our X-ray photoemission studies, we argue that the pseudobrookite phase apparently consists mainly of FeTi_2O_5 , rather than the expected Fe_2TiO_5 phase. The structure and the optical properties of the films exhibit negligible changes on vacuum annealing, although this strongly affects the magnetization and the electrical conductivity. On vacuum annealing, both the FeTiO_3 and $\text{Fe}_{1.4}\text{Ti}_{0.6}\text{O}_3$ films show a large increase in saturation magnetization, reaching nearly $0.04 \mu_{\text{B}}/\text{Fe}$ for the Fe-rich films. We attribute this ferromagnetism to oxygen vacancy defect mediated effects, with only a small contribution arising from the interfacial magnetism observed in ilmenite-hematite structures. The optical band gap of both samples is 2.0 eV, and this value is almost unchanged on vacuum annealing. These results suggest that the ferromagnetic signal in iron titanate composites may also be strongly affected by oxygen stoichiometry, and that the magnitude of the saturation magnetization depends on the Fe:Ti ratio in the films. While the lamellar magnetism in ilmenite-hematite films arising from different Fe valence states at the interface provides a much larger magnetization than we observe in the oxygen deficient ilmenite-pseudobrookite films, vacuum annealing may provide another avenue for tuning the magnetic and electrical properties of FeTiO_3 based materials beyond controlling the inhomogeneous sample structure.

ACKNOWLEDGMENTS

The authors dedicate the manuscript to the memory of late Professor Gavin Lawes, and acknowledge support for this research provided by the National Science Foundation through DMR 1006381 and the Jane and Frank Warchol Foundation.

¹S. A. Wolf, D. D. Awschalom, R. A. Buhrman, J. M. Daughton, S. von Molnar, M. L. Roukes, A. Y. Chtchelkanova, and D. M. Treger, *Science* **294**(5546), 1488–1495 (2001).

²D. B. Bucholz, R. P. H. Chang, J. H. Song, and J. B. Ketterson, *Appl. Phys. Lett.* **87**, 082504 (2005).

³S. A. Chambers *et al.*, *Appl. Phys. Lett.* **82**, 1257 (2003).

⁴J. M. D. Coey, *Curr. Opin. Solid State Mater. Sci.* **10**(2), 83–92 (2006).

- ⁵T. Dietl, H. Ohno, F. Matsukura, J. Cibert, and D. Ferrand, *Science* **287**, 1019 (2000).
- ⁶R. Janisch, P. Gopal, and N. Spaldin, *J. Phys.: Condens. Matter* **17**, R657 (2005).
- ⁷G. Lawes, A. S. Risbud, A. P. Ramirez, and R. Seshadri, *Phys. Rev. B* **71**(4), 45201 (2005).
- ⁸A. Manivannan, M. S. Seehra, S. B. Majumder, and R. S. Katiyar, *Appl. Phys. Lett.* **83**, 111 (2003).
- ⁹Y. Matsumoto, M. Murakami, T. Shono, T. Hasegawa, T. Fukumura, M. Kawasaki, P. Ahmet, T. Chikyow, S. Koshihara, and H. Koinuma, *Science* **291**, 854 (2001).
- ¹⁰H. Nguyen Hoa, J. Sakai, H. Ngo Thu, and V. Brize, *J. Magn. Magn. Mater.* **302**(1), 228–231 (2006).
- ¹¹K. Ueda, H. Tabata, and T. Kawai, *Appl. Phys. Lett.* **79**, 988 (2001).
- ¹²H. Nguyen Hoa, J. Sakai, N. Poirot, and V. Brize, *Phys. Rev. B: Condens. Matter Mater. Phys.* **73**(13), 132404 (2006).
- ¹³R. P. Panguluri, P. Kharel, C. Sudakar, R. Naik, R. Suryanarayanan, V. M. Naik, A. G. Petukhov, B. Nadgorny, and G. Lawes, *Phys. Rev. B: Condens. Matter Mater. Phys.* **79**(16), 165208 (2009).
- ¹⁴Y. Takada, M. Nakanishi, T. Fujii, and J. Takada, *J. Magn. Magn. Mater.* **310**(2), 2108–2110 (2007).
- ¹⁵R. Pentcheva and H. S. Nabi, *Phys. Rev. B: Condens. Matter Mater. Phys.* **77**(17), 172405–172401 (2008).
- ¹⁶P. Robinson, R. J. Harrison, S. A. McEnroe, and R. B. Hargraves, *Nature* **418**(6897), 517–520 (2002).
- ¹⁷H. S. Nabi, R. J. Harrison, and R. Pentcheva, *Phys. Rev. B: Condens. Matter Mater. Phys.* **81**(21), 214432 (2010).
- ¹⁸S. Yan, S. Ge, W. Qiao, and Y. Zuo, *J. Magn. Magn. Mater.* **322**(7), 824–826 (2010).
- ¹⁹K. Rode, R. D. Gunning, R. G. S. Sofin, M. Venkatesan, J. G. Lunney, J. M. D. Coey, and I. V. Shvets, *J. Magn. Magn. Mater.* **320**(23), 3238–3241 (2008).
- ²⁰Y. Ishikawa, *J. Phys. Soc. Jpn.* **13**, 1298–1310 (1958).
- ²¹D. S. Ginley and M. A. Butler, *J. Appl. Phys.* **48**(5), 2019–2021 (1977).
- ²²Z. Dai, H. Naramoto, K. Narumi, S. Yamamoto, and A. Miyashita, *J. Appl. Phys.* **85**(10), 7433–7437 (1999).
- ²³T. Fujii, Y. Takada, M. Nakanishi, J. Takada, M. Kimura, and H. Yoshikawa, paper presented at the 17th International Vacuum Congress (IVC-17), 13th International Conference on Surface Science (ICSS-13) and International Conference on Nanoscience and Technology (ICN+T 2007), 2–6 July 2007, United Kingdom, 2008.
- ²⁴Z. Dai, P. Zhu, S. Yamamoto, A. Miyashita, K. Narum, and H. Naramoto, *Thin Solid Films* **339**(1–2), 114–116 (1999).
- ²⁵T. Fujii, M. Kayano, Y. Takada, M. Nakanishi, and J. Takada, paper presented at the 15th International Symposium on the Reactivity of Solids (ISRS), 9–13 November 2003, Netherlands, 2004.
- ²⁶E. Popova, B. Warot-Fonrose, H. Ndimabaka, M. Bibes, N. Keller, B. Berini, K. Bouzouane, and Y. Dumont, *J. Appl. Phys.* **103**(9), 093909 (2008).
- ²⁷X. Fu, Y. Wang, and F. Wei, *Metal. Mater. Trans. A* **41**, 1338–1348 (2010).
- ²⁸D. Bersani, P. P. Lottici, and A. Montenero, *J. Mater. Sci.* **35**(17), 4301–4305 (2000).
- ²⁹M. Macek, B. Orel, and T. Meden, *J. Sol-Gel Sci. Technol.* **8**(1–3), 771–779 (1997).
- ³⁰J. K. Srivastava, W. Treutmann, and E. Untersteller, *Phys. Rev. B: Condens. Matter Mater. Phys.* **68**(14), 144404 (2003).
- ³¹R. G. Teller, M. R. Antonio, A. E. Grau, M. Gueguin, and E. Kostiner, *J. Solid State Chem.* **88**(2), 334–350 (1990).
- ³²X. Wu, G. Steinle-Neumann, O. Narygina, I. Kantor, C. McCammon, V. Prakashenka, V. Swamy, and L. Dubrovinsky, *Phys. Rev. Lett.* **103**(6), 065503 (2009).
- ³³R. K. Pandey, P. Padmini, R. Schadt, J. Dou, H. Stern, R. Wilkins, R. Dwivedi, W. J. Geerts, and C. O'Brien, *J. Electroceram.* **22**(1–3), 334–341 (2009).
- ³⁴F. J. Berry, J. F. Marco, S. J. Stewart, and H. M. Widatallah, *Solid State Commun.* **117**(4), 235–238 (2001).
- ³⁵M. Li-Jian, C. P. Moreira de Sa, and M. P. dos Santos, *Appl. Surf. Sci.* **78**(1), 57–61 (1994).
- ³⁶A. T. Raghavender, N. H. Hong, K. J. Lee, M.-H. Jung, Z. Skoko, M. Vasilevskiy, M. F. Cerqueira, and A. P. Samantilleke, *J. Magn. Magn. Mater.* **331**, 129–132 (2013).